



Measurement of D_s^\pm production asymmetry in pp collisions at $\sqrt{s} = 7$ and 8 TeV

LHCb collaboration[†]

Abstract

The inclusive D_s^\pm production asymmetry is measured in pp collisions collected by the LHCb experiment at centre-of-mass energies of $\sqrt{s} = 7$ and 8 TeV. Promptly produced D_s^\pm mesons are used, which decay as $D_s^\pm \rightarrow \phi\pi^\pm$, with $\phi \rightarrow K^+K^-$. The measurement is performed in bins of transverse momentum, p_T , and rapidity, y , covering the range $2.5 < p_T < 25.0$ GeV/ c and $2.0 < y < 4.5$. No kinematic dependence is observed. Evidence of nonzero D_s^\pm production asymmetry is found with a significance of 3.3 standard deviations.

Published in JHEP 08 (2018) 008

© 2018 CERN for the benefit of the LHCb collaboration. CC-BY-4.0 licence.

[†]Authors are listed at the end of this paper.

1 Introduction

At LHC energies, $c\bar{c}$ quark pairs are copiously produced in pp collisions with a total cross-section at a centre-of-mass energy of 7 TeV of $\sigma_{c\bar{c}} = 1419 \pm 136 \mu\text{b}$ [1]. The subsequent hadronisation process can introduce a charge asymmetry in the production of charm hadrons. This asymmetry is influenced by the valence quarks of the colliding protons, which results in a preference for the \bar{c} quark to form a meson, *e.g.* a D^- or \bar{D}^0 meson. A c quark, on the other hand, can form charm baryons, *e.g.* a Λ_c^+ baryon, with the proton's valence quarks. This difference in hadronisation gives rise to different kinematic distributions between charge-conjugated charm hadrons, and therefore results in a charge asymmetry.

The D_s^+ meson does not contain any of the proton's valence quarks, which means that the aforementioned processes can contribute only indirectly to a production asymmetry. The D_s^+ production asymmetry is defined as

$$A_P(D_s^+) = \frac{\sigma(D_s^+) - \sigma(D_s^-)}{\sigma(D_s^+) + \sigma(D_s^-)}, \quad (1)$$

where $\sigma(D_s^\pm)$ is the inclusive prompt production cross-section. It is difficult to make accurate predictions of the D_s^+ production asymmetry due to the nonperturbative nature of the hadronisation process. Nonetheless, the Lund string fragmentation model [2], implemented in PYTHIA [3], describes hadronisation that can give rise to production asymmetries for heavy flavours [4–6]. This model predicts that production asymmetries can be dependent on kinematics due to interactions with the beam remnants. A measurement of the D_s^+ production asymmetry can be used to test nonperturbative QCD models and is an essential input for measurements of direct CP violation in the decays of D_s^+ mesons in LHCb.

This paper presents a measurement of the D_s^+ production asymmetry in pp collisions using two data sets corresponding to integrated luminosities of 1.0 fb^{-1} and 2.0 fb^{-1} , recorded by the LHCb detector at centre-of-mass energies of 7 and 8 TeV in 2011 and 2012, respectively. An inclusive sample of promptly produced D_s^+ mesons in the decay mode $D_s^+ \rightarrow \phi\pi^+$ is used, where $\phi \rightarrow K^+K^-$. This sample includes excited states that decay to D_s^+ mesons, such as D_s^{*+} mesons which decay to $D_s^+\gamma$ or $D_s^+\pi^0$. The inclusion of charge-conjugate processes is implied throughout this paper, except in the definition of the asymmetries.

The D_s^+ production asymmetries derived from PYTHIA are compared to the results obtained in this paper. A previous measurement by the LHCb collaboration [7] with the 7 TeV data set indicated a small excess of D_s^- over D_s^+ mesons, resulting in a negative value for the production asymmetry. This paper, with improvements in the detector calibration, supersedes the previous measurement and includes the 8 TeV data set.

2 Detector and simulation

The LHCb detector [8, 9] is a single-arm forward spectrometer covering the pseudorapidity range $2 < \eta < 5$, designed for the study of particles containing b or c quarks. The detector includes a high-precision tracking system consisting of a silicon-strip vertex detector surrounding the pp interaction region, a large-area silicon-strip detector located upstream

of a dipole magnet with a bending power of about 4 Tm, and three stations of silicon-strip detectors and straw drift tubes placed downstream of the magnet. The polarity of the dipole magnet is reversed periodically throughout data taking and the corresponding data sets (referred to as *MagUp* and *MagDown*) are approximately equal in size. The tracking system provides a measurement of momentum, p , of charged particles with a relative uncertainty that varies from 0.5% at low momentum to 1.0% at 200 GeV/ c . The minimum distance of a track to a primary vertex (PV), the impact parameter (IP), is measured with a resolution of $(15 + 29/p_T)$ μm , where p_T is the component of the momentum transverse to the beam, in GeV/ c . Different types of charged hadrons are distinguished using information from two ring-imaging Cherenkov detectors. Photons, electrons and hadrons are identified by a calorimeter system consisting of scintillating-pad and preshower detectors, an electromagnetic calorimeter and a hadronic calorimeter. Muons are identified by a system composed of alternating layers of iron and multiwire proportional chambers. The online event selection is performed by a trigger [10], which consists of a hardware stage, based on information from the calorimeter and muon systems, followed by a software stage, which applies a full event reconstruction.

In the simulation, which is used for comparing the production asymmetry results, pp collisions are generated using PYTHIA [3], which has implemented the Lund string fragmentation model [2], with a specific LHCb configuration [11]. Decays of hadronic particles are described by EVTGEN [12], in which final-state radiation is generated using PHOTOS [13]. The interaction of the generated particles with the detector, and its response, are implemented using the GEANT4 toolkit [14] as described in Ref. [15].

3 Data selection

Signal candidates are selected by the requirements made in the trigger and in the offline selection. At the hardware trigger stage, events are required to have a muon with high transverse momentum or a hadron, photon or electron with high transverse energy deposited in the calorimeters. The software trigger requires at least one charged particle that has $p_T > 1.7 \text{ GeV}/c$ at 7 TeV or $p_T > 1.6 \text{ GeV}/c$ at 8 TeV, and is inconsistent with originating from any PV. Subsequently, three well reconstructed tracks are required to originate from a common vertex with a significant displacement from any PV. Additional requirements are made to select three-prong decays with an invariant mass close to that of the D_s^+ meson. The reconstructed D_s^+ meson must have $p_T > 2.5 \text{ GeV}/c$.

In the offline selection, trigger decisions are associated with reconstructed tracks or energy deposits. Requirements can therefore be made on whether the trigger decision was due to the signal candidate, other particles in the event, or a combination of both. For the hardware trigger stage, a positive trigger decision is required to be caused by a particle that is distinct from any of the final-state particles that compose the D_s^+ candidate. This requirement is independent of whether or not the signal candidate itself also caused a positive trigger decision, and is therefore referred to as triggered independently of signal (TIS) [10]. For the software trigger stage, the positive trigger decision is required to be associated with the final-state particles of the D_s^+ candidate. This is called triggered on signal (TOS) [10].

The three tracks from the final-state particles are required to not point back to any PV. To reduce candidates from b -hadron decays, the D_s^+ candidate itself must point to a

PV. Its decay vertex is required to have a good quality and to be significantly displaced from any PV. To ensure a good overlap with the additional samples used for calibration purposes, $p > 5.0$ (3.0) GeV/ c and $p_T > 400$ (300) MeV/ c are required for the pions (kaons). Background due to random combinations of tracks is suppressed by requiring the sum of the p_T of the final-state tracks to be larger than 2.8 GeV/ c .

Kaon and pion mass assignments to the particle tracks are based on the particle identification (PID) information obtained primarily from the Cherenkov detectors. The invariant mass of the kaon pair is required to be within 20 MeV/ c^2 of the known ϕ mass [16]. The mass of the D_s^+ candidate is selected to be between 1900 and 2035 MeV/ c^2 . Additional PID and mass requirements are applied to suppress two particular sources of background. The first comes from $\Lambda_c^+ \rightarrow pK^-\pi^+$ decays, where the proton is misidentified as a kaon. The second are $D^+ \rightarrow K^-\pi^+\pi^+$ decays, where one of the pions is misidentified as a kaon. Both of these are suppressed by applying tighter PID requirements in a small window of invariant mass of the corresponding particle combination around the known Λ_c^+ and D^+ masses. The remaining contribution from misidentified Λ_c^+ and D^+ decays is negligibly small.

After the full selection, 2.9×10^6 and 9.1×10^6 D_s^+ candidates are selected in the 7 TeV and 8 TeV data sets, respectively, with a signal purity of 97%. The increase for the 8 TeV data set is not only due to a higher integrated luminosity, but also to improvements in the trigger. The fraction of events with more than one candidate, which are not removed in this analysis, is only 2×10^{-4} , resulting in a negligible bias in the final asymmetry. The two data sets with opposite magnetic fields are analysed separately.

4 Analysis method

The raw asymmetry is defined as the difference between the observed numbers, $N(D_s^\pm)$, of D_s^+ and D_s^- mesons

$$A_{\text{raw}} = \frac{N(D_s^+) - N(D_s^-)}{N(D_s^+) + N(D_s^-)}. \quad (2)$$

This asymmetry must be corrected for contributions from D_s^+ mesons originating from b -hadron decays, and for detection asymmetries, A_D . The production asymmetry, assuming the CP asymmetry in Cabibbo-favoured D_s^+ decays to be negligible at the precision of this measurement, is determined as

$$A_P(D_s^+) = \frac{1}{1 - f_{\text{bkg}}} (A_{\text{raw}} - A_D - f_{\text{bkg}} A_P(B)), \quad (3)$$

where f_{bkg} is the fraction of D_s^+ mesons that originate from b -hadron decays and $A_P(B)$ the production asymmetry of these b hadrons.

Since the production asymmetry may depend on the kinematics of the D_s^+ meson, the measurement is performed in two-dimensional bins of p_T and rapidity, y . Four bins in p_T and three bins in y are chosen as follows

$$\begin{aligned} p_T \text{ [GeV}/c] : & [2.5, 4.7]; [4.7, 6.5]; [6.5, 8.5]; [8.5, 25.0], \\ y : & [2.0, 3.0]; [3.0, 3.5]; [3.5, 4.5], \end{aligned}$$

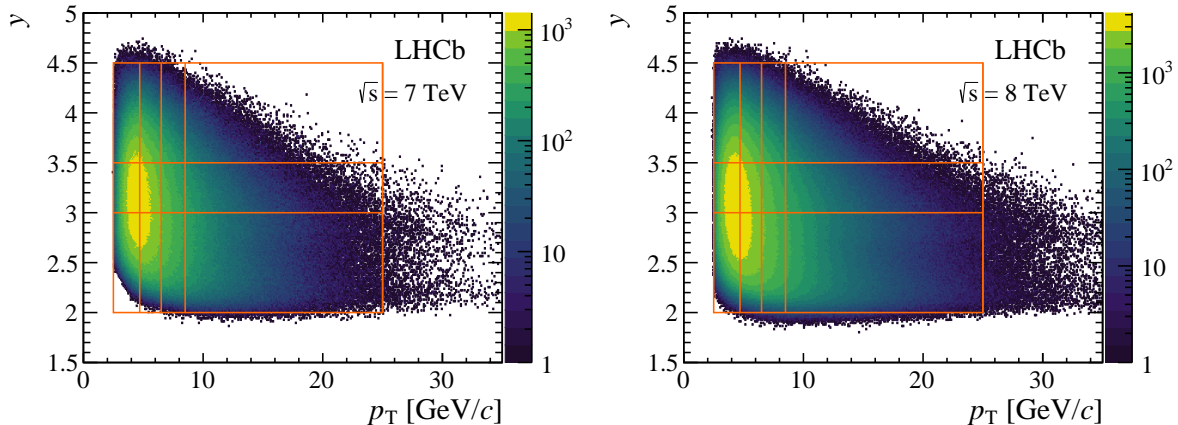


Figure 1: Distribution of D_s^+ candidates for the $\sqrt{s} = 7$ and 8 TeV data sets as a function of p_T and y . The binning scheme used for the $A_P(D_s^+)$ measurement is overlaid.

where the rapidity of the D_s^+ meson is defined as

$$y = \frac{1}{2} \ln \left(\frac{E + p_z c}{E - p_z c} \right). \quad (4)$$

Here, E is the energy of the D_s^+ meson and p_z the component of its momentum along the beam direction. This binning scheme is chosen such that the bins are roughly equally populated and is the same as that used for the previous $A_P(D_s^+)$ measurement [7], except that the lowest p_T bin is now split into two. The two-dimensional distribution in p_T and y of D_s^+ candidates is shown in Fig. 1 along with the binning scheme.

4.1 Measurement of raw asymmetries

The signal yields and asymmetries are obtained from binned maximum-likelihood fits to the D_s^+ mass distributions in the twelve kinematic bins, separately for the two data-taking periods and the two magnet polarities. The signal component is modelled with a Hypatia function with tails on both sides [17], and the combinatorial background, from random combinations of tracks, with an exponential function. The parameters describing the tails of the Hypatia function are determined by fits to the D_s^+ mass distributions that are performed in each kinematic bin, in which the data sets from 7 and 8 TeV and both magnet polarities are combined. These parameters are then kept fixed in the fits to obtain the raw asymmetries. The raw asymmetries in each kinematic bin are obtained from simultaneous fits to the D_s^+ and D_s^- mass distributions in which all free parameters are shared, except for the yields, the mean mass of the signal component, and the background parameters. The mean mass can be different as the momentum reconstruction may have different biases for positive and negative tracks. The variation of the background parameters is needed to account for potential asymmetries in the background. Two example fits are shown in Fig. 2.

A systematic uncertainty is assigned for the effect of fixing the tail parameters by varying their values and reassessing the raw asymmetries. In addition, a possible bias from the fit model is studied by generating invariant mass distributions with the signal component described by a double Gaussian function with power-law tails on both sides,

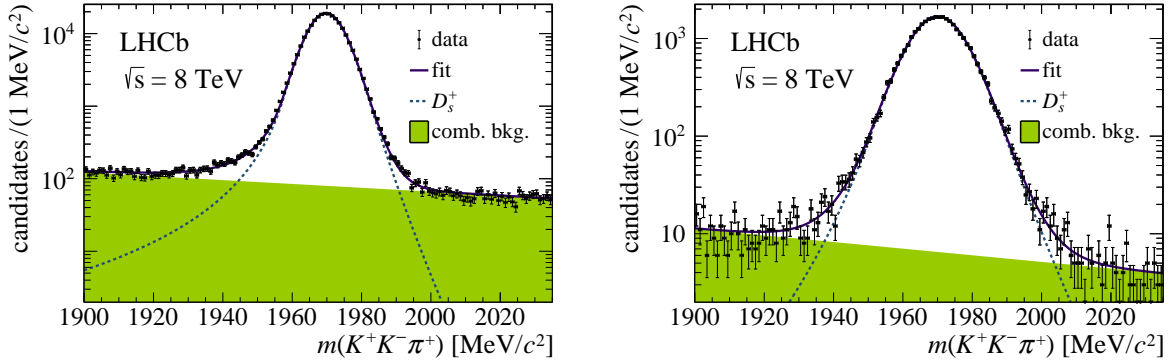


Figure 2: Invariant mass distribution of the D_s^+ candidates in the kinematic range (left) $2.0 < y < 3.0$ and $2.5 < p_T < 4.7 \text{ GeV}/c$, and (right) $3.5 < y < 4.5$ and $8.5 < p_T < 25.0 \text{ GeV}/c$ for the $\sqrt{s} = 8 \text{ TeV}$ data set recorded with *MagDown*. Also shown is the result of the fit, indicating the signal and combinatorial background.

which are subsequently fitted using the default Hypatia function. The differences in the raw asymmetry for both studies are assigned as a systematic uncertainty. This is small because the low amount of combinatorial background allows for little bias from the fit model.

4.2 Contribution from b -hadron decays

An estimate of the fraction of D_s^+ candidates from b -hadron (B^+ , B^0 , B_s^0 , Λ_b^0) decays is performed using a combination of simulation, known cross-sections [18, 19] and known branching fractions [16]. Simulation samples are used to determine the reconstruction and selection efficiencies relative to those for the signal decay. The fraction of D_s^+ from b -hadron decays is estimated to be $f_{\text{bkg}} = (4.12 \pm 1.23)\%$, where the uncertainty includes contributions from the experimental input and the simulation.

The production asymmetries for b hadrons are taken from measurements from the LHCb collaboration [20–22]. The B_s^0 production asymmetry is diluted due to the fact that, before it decays, a B_s^0 meson oscillates with high frequency to a \bar{B}_s^0 , and vice versa. Hence, its contribution is assumed to be zero. Wherever multiple LHCb measurements are available using different decay channels, their results are combined in a weighted average. The contribution of the background asymmetry to $A_P(D_s^+)$, as defined in Eq. 3, is found to be

$$\begin{aligned} f_{\text{bkg}} A_P(B) &= (0.3 \pm 1.0) \times 10^{-4} \text{ at } 7 \text{ TeV}, \\ f_{\text{bkg}} A_P(B) &= (1.7 \pm 0.8) \times 10^{-4} \text{ at } 8 \text{ TeV}, \end{aligned}$$

which is very small compared to the experimental precision of the measurement. The dilution from f_{bkg} in the denominator of Eq. 3 gives a small correction to A_{raw} .

5 Detection asymmetries

Detection asymmetries are caused by the differences in reconstruction efficiencies between D_s^+ and D_s^- mesons and originate from the various stages in the reconstruction process.

Table 1: Raw and detection asymmetries in percent, for the 7 and 8 TeV data sets. The detection asymmetries are determined on the data combined from all kinematic bins. The first uncertainty is statistical, the second systematic.

source	$\sqrt{s} = 7 \text{ TeV}$	$\sqrt{s} = 8 \text{ TeV}$
A_{raw}	$-0.431 \pm 0.061 \pm 0.006$	$-0.492 \pm 0.034 \pm 0.006$
A_{track}^{π}	$0.093 \pm 0.096 \pm 0.048$	$-0.026 \pm 0.068 \pm 0.048$
A_{track}^{KK}	$0.000 \pm 0.000 \pm 0.030$	$0.000 \pm 0.000 \pm 0.030$
A_{PID}	$-0.018 \pm 0.008 \pm 0.012$	$0.008 \pm 0.005 \pm 0.012$
$A_{\text{trigger}}^{\text{hardware}}$	$0.139 \pm 0.229 \pm 0.066$	$-0.060 \pm 0.115 \pm 0.066$
$A_{\text{trigger}}^{\text{software}}$	$-0.005 \pm 0.018 \pm 0.033$	$0.026 \pm 0.011 \pm 0.033$
$A_{\text{P}}(D_s^+)$	$-0.671 \pm 0.267 \pm 0.095$	$-0.477 \pm 0.145 \pm 0.095$

Since these asymmetries are small, they factorise and can be added up as

$$A_{\text{D}} = A_{\text{track}}^{\pi} + A_{\text{track}}^{KK} + A_{\text{PID}} + A_{\text{trigger}}^{\text{software}} + A_{\text{trigger}}^{\text{hardware}}. \quad (5)$$

Here, A_{track}^{π} and A_{track}^{KK} are the tracking asymmetries of the pion and the kaon pair, respectively. The asymmetry originating from the PID requirements in the selection is denoted by A_{PID} . Lastly, asymmetries arising from the trigger are split between the hardware and software components of the trigger as $A_{\text{trigger}}^{\text{hardware}}$ and $A_{\text{trigger}}^{\text{software}}$. All detection asymmetries are determined for and applied to each bin using data-driven methods described below, and corrected by simulations wherever necessary. Values of the detection asymmetries for the 7 and 8 TeV data sets, determined on the data combined from all kinematic bins, are listed in Table 1. In this paper, the statistical uncertainties from the detection asymmetries, obtained from control samples, are included in the total statistical uncertainty of the measurement.

5.1 Tracking asymmetries

When the kaons originate from the ϕ resonance, there can be no detection asymmetry from the kaon pair. Only the small fraction of kaons coming from the nonresonant decays included in the selection can introduce a detection asymmetry, and only when the kinematic distributions of the two oppositely charged kaons are different. In general, the reconstruction efficiency of kaons suffers from a sizeable difference between the interaction cross-sections of K^+ and K^- mesons with the detector material, which depends on the kaon momentum. For the pair of kaons, however, these differences largely cancel, since the momentum distributions of the positively and negatively charged kaons are very similar. An upper limit of 3×10^{-4} is set on their contribution, based on their kinematic overlap and the maximum kaon detection asymmetry as measured with calibration data [23, 24].

The pion tracking asymmetry is determined using two different methods, analogously to Ref. [24]. The first uses muons from partially reconstructed $J/\psi \rightarrow \mu^+ \mu^-$ decays, as described in Ref. [25]. The second method uses partially reconstructed $D^{*+} \rightarrow D^0 \pi^+$ decays with $D^0 \rightarrow K^- \pi^+ \pi^- \pi^+$, where one of the pions from the D^0 decay does not need

to be reconstructed [7]. Both methods have limitations: the former because it does not probe the full detector acceptance or the effect of the hadronic interaction of the pion with the detector material, the latter because it is limited to pions with momenta below 100 GeV/c. The limitations on the $J/\psi \rightarrow \mu^+\mu^-$ method are assessed and corrected using simulation. After these corrections, the two methods are in good agreement and the final value of A_{track}^π is determined by the weighted average of the two methods. For pions with $p > 100 \text{ GeV}/c$, A_{track}^π is determined solely using the $J/\psi \rightarrow \mu^+\mu^-$ method combined with the above-mentioned corrections.

5.2 Particle identification asymmetries

The asymmetry induced by the PID requirements, A_{PID} , is determined using large samples of $D^{*+} \rightarrow D^0\pi^+$ decays, with $D^0 \rightarrow K^-\pi^+$ [26]. The D^{*+} charge identifies which of the two particles is the kaon and which the pion in the D^0 decay without the use of PID requirements. These unbiased samples are then used to determine the PID efficiencies and corresponding charge asymmetries.

5.3 Trigger asymmetries

The efficiencies of the hardware and software triggers are studied using the signal sample of prompt $D_s^+ \rightarrow K^+K^-\pi^+$ decays. For the hardware trigger, the TIS asymmetry is determined with respect to decays that are TOS as well as TIS. This is done by evaluating the TIS asymmetry separately for candidates that are TOS, triggered by the K^+ track, and candidates that are TOS, triggered by the K^- track, and then averaging the asymmetry. Due to possible correlations between the signal decay and the rest of the event, this method is biased. In addition, as a result of the coarse transverse segmentation of the hadronic calorimeter, the energy deposited by other particles in the event can increase the energy that is measured and associated to the signal tracks of TOS events. This further increases the bias of the measured TIS asymmetry. To assess the systematic uncertainty from this method, a much larger sample of $D^+ \rightarrow K^-\pi^+\pi^+$ decays is studied. In this sample the TIS asymmetries are determined using candidates that are TOS, triggered by one, two or all three of the final-state particles. The difference in the asymmetry resulting from these variations is assigned as the systematic uncertainty.

The asymmetry due to the software trigger is assessed by the TOS efficiency of a single track from the $K^+K^-\pi^+$ final state in events that have been triggered by one of the other tracks. The individual efficiencies are determined in bins of transverse momentum and pseudorapidity, and are then combined to obtain the overall asymmetry introduced by the software trigger selection. The systematic uncertainty is determined by studying the effect of the difference between the online and offline determination of the transverse momentum, and by determining the effect of the binning scheme.

5.4 Systematic uncertainties

In addition to the systematic uncertainties discussed above, all detection asymmetries are determined in bins of kinematic variables of final-state particles, for example p_T , η . The limitations of the binning schemes are evaluated by changing to different binning schemes, *e.g.* p , η . The systematic uncertainties are fully correlated between the 7 TeV and 8 TeV

data sets. An overview of the systematic and statistical uncertainties for both data sets from the various sources of detection asymmetries is shown in Table 1.

6 Results

The values of the D_s^+ production asymmetry obtained using the *MagUp* and *MagDown* data sets separately are compatible with each other in each kinematic bin within two standard deviations, as illustrated in Fig. 4 in the Appendix. The two magnet polarities are combined using the arithmetic mean to ensure that any residual magnet-polarity-dependent detection asymmetry cancels. Due to the small difference in centre-of-mass energy and since the observed production asymmetries are statistically compatible, the 7 TeV and 8 TeV data sets are combined in a weighted average, maximising the statistical precision. The resulting production asymmetries in each kinematic bin are presented in Table 2. The results for both centre-of-mass energies separately are provided in Tables 3 and 4 in the Appendix.

Since no kinematic dependence is observed, the data from all kinematic bins are combined and the full procedure is repeated to obtain values equivalent to a weighted average based on the signal yields, taking into account the correlations from the calibration samples between the kinematic bins. These are shown for the 7 and 8 TeV data sets separately in Table 1. Taking the weighted average of these two results with the systematic uncertainties as fully correlated, the combined value is

$$A_P(D_s^+) = (-0.52 \pm 0.13 (\text{stat}) \pm 0.10 (\text{syst}))\%,$$

corresponding to a deviation of 3.3σ from the hypothesis of no production asymmetry.

The results presented here are in agreement with the previous measurement of the D_s^+ production asymmetry [7], obtained using only the 7 TeV data set. A cross-check is performed by measuring $A_P(D_s^+)$ in two other disjoint regions in the $D_s^+ \rightarrow K^+ K^- \pi^+$ Dalitz plot, analogous to those defined in Ref. [24]. These are the region including the $K^*(892)^0$ resonance, and the remaining nonresonant region. The $A_P(D_s^+)$ measurements

Table 2: Values of the D_s^+ production asymmetry in percent, including, respectively, the statistical and systematic uncertainties for each of the D_s^+ kinematic bins using the combined $\sqrt{s} = 7$ and 8 TeV data sets. The statistical and systematic uncertainties include the corresponding contributions from the detection asymmetries, and are therefore correlated between the bins.

p_T [GeV/c]	y		
	2.0 – 3.0	3.0 – 3.5	3.5 – 4.5
2.5 – 4.7	$-0.63 \pm 0.34 \pm 0.32$	$-0.66 \pm 0.31 \pm 0.13$	$-0.65 \pm 0.33 \pm 0.14$
4.7 – 6.5	$-0.68 \pm 0.25 \pm 0.27$	$-0.06 \pm 0.26 \pm 0.10$	$-0.72 \pm 0.26 \pm 0.13$
6.5 – 8.5	$-0.55 \pm 0.22 \pm 0.06$	$-0.57 \pm 0.26 \pm 0.10$	$-0.48 \pm 0.30 \pm 0.17$
8.5 – 25.0	$-0.40 \pm 0.15 \pm 0.08$	$-0.24 \pm 0.22 \pm 0.10$	$-0.86 \pm 0.33 \pm 0.09$

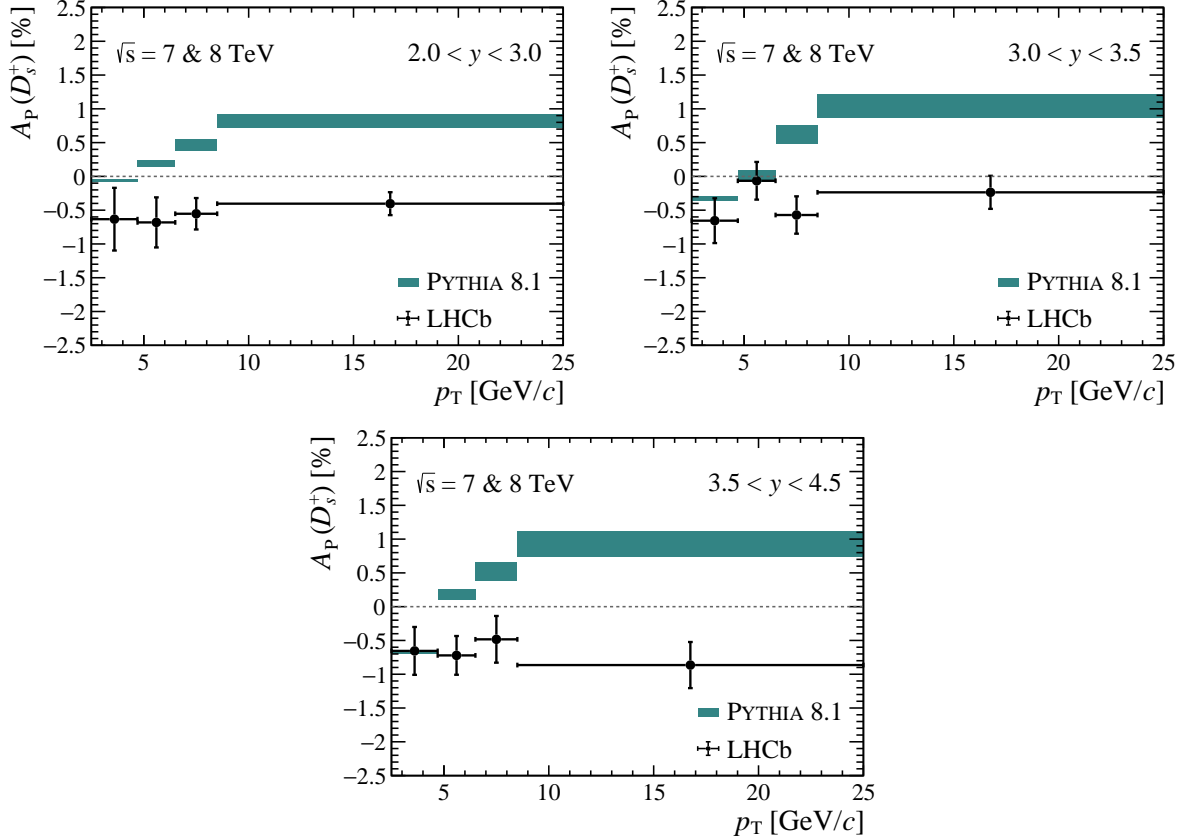


Figure 3: Results of the LHCb measurement of the D_s^+ production asymmetry as a function of p_T for three different bins of rapidity, compared to the results from PYTHIA. Both are for the combined $\sqrt{s} = 7$ and 8 TeV data sets. The uncertainties on the PYTHIA predictions are statistical only.

in the three regions are in good agreement in all kinematic bins. However, these regions are not included in the measurement of $A_P(D_s^+)$, since it was found that including them slightly increases the uncertainty on the measurement due to the larger systematic effects from the detection asymmetries.

6.1 Comparison with PYTHIA predictions

The PYTHIA event generator includes models for mechanisms that cause production asymmetries [4–6]. The results obtained in this paper are compared with production asymmetries obtained from PYTHIA 8.1 [3] with the CT09MCS set of parton density functions [27]. In this configuration, which is the default LHCb tuning of PYTHIA, events containing a D_s^+ meson are extracted from generated minimum bias interactions as described in Ref. [11]. The results of this comparison are shown in Fig. 3 as a function of p_T in the different y bins for the combined 7 and 8 TeV data sets, and separately for 7 and 8 TeV in Fig. 5 in the Appendix. The PYTHIA simulation shows a strong dependence on both p_T and y , whereas the measurements presented here do not.

7 Summary and conclusions

A measurement of the D_s^+ production asymmetry is performed in pp collisions at centre-of-mass energies of 7 and 8 TeV. The measurement is carried out in bins of transverse momentum and rapidity, covering the range $2.5 < p_T < 25.0$ GeV/ c and $2.0 < y < 4.5$, using $D_s^+ \rightarrow K^+ K^- \pi^+$ decays, where the kaon pair is created via the ϕ resonance. The production asymmetry measured in bins of p_T and y is shown in Fig. 3. No kinematic dependence is observed, contrary to expectations from simulations with the PYTHIA event generator.

The results are in agreement with the previous result from the LHCb collaboration [7], which was performed on the data recorded at 7 TeV only. This updated measurement, with improvements in the detector calibration, supersedes the previous result and provides evidence for a nonzero value for the production asymmetry with a significance of 3.3 standard deviations. The results presented in this paper can be used as input to tune the parameters of production models in different event generators.

Acknowledgements

We express our gratitude to our colleagues in the CERN accelerator departments for the excellent performance of the LHC. We thank the technical and administrative staff at the LHCb institutes. We acknowledge support from CERN and from the national agencies: CAPES, CNPq, FAPERJ and FINEP (Brazil); MOST and NSFC (China); CNRS/IN2P3 (France); BMBF, DFG and MPG (Germany); INFN (Italy); NWO (The Netherlands); MNiSW and NCN (Poland); MEN/IFA (Romania); MinES and FASO (Russia); MinECo (Spain); SNSF and SER (Switzerland); NASU (Ukraine); STFC (United Kingdom); NSF (USA). We acknowledge the computing resources that are provided by CERN, IN2P3 (France), KIT and DESY (Germany), INFN (Italy), SURF (The Netherlands), PIC (Spain), GridPP (United Kingdom), RRCKI and Yandex LLC (Russia), CSCS (Switzerland), IFIN-HH (Romania), CBPF (Brazil), PL-GRID (Poland) and OSC (USA). We are indebted to the communities behind the multiple open-source software packages on which we depend. Individual groups or members have received support from AvH Foundation (Germany), EPLANET, Marie Skłodowska-Curie Actions and ERC (European Union), ANR, Labex P2IO and OCEVU, and Région Auvergne-Rhône-Alpes (France), Key Research Program of Frontier Sciences of CAS, CAS PIFI, and the Thousand Talents Program (China), RFBR, RSF and Yandex LLC (Russia), GVA, XuntaGal and GENCAT (Spain), Herchel Smith Fund, the Royal Society, the English-Speaking Union and the Leverhulme Trust (United Kingdom).

Results for separate data sets

Table 3: Values of the D_s^+ production asymmetry in percent, including, respectively, the statistical and systematic uncertainty for each of the D_s^+ kinematic bins using the $\sqrt{s} = 7$ TeV data set.

p_T [GeV/c]	y		
	2.0 – 3.0	3.0 – 3.5	3.5 – 4.5
2.5 – 4.7	$-0.74 \pm 0.62 \pm 0.32$	$-1.34 \pm 0.55 \pm 0.13$	$-1.15 \pm 0.60 \pm 0.14$
4.7 – 6.5	$-0.54 \pm 0.51 \pm 0.27$	$0.16 \pm 0.49 \pm 0.10$	$-0.70 \pm 0.48 \pm 0.13$
6.5 – 8.5	$-1.05 \pm 0.40 \pm 0.06$	$-0.76 \pm 0.47 \pm 0.10$	$-0.68 \pm 0.56 \pm 0.17$
8.5 – 25.0	$-0.14 \pm 0.32 \pm 0.08$	$-0.00 \pm 0.43 \pm 0.10$	$-1.18 \pm 0.63 \pm 0.09$

Table 4: Values of the D_s^+ production asymmetry in percent, including, respectively, the statistical and systematic uncertainty for each of the D_s^+ kinematic bins using the $\sqrt{s} = 8$ TeV data set.

p_T [GeV/c]	y		
	2.0 – 3.0	3.0 – 3.5	3.5 – 4.5
2.5 – 4.7	$-0.59 \pm 0.40 \pm 0.32$	$-0.34 \pm 0.37 \pm 0.13$	$-0.45 \pm 0.39 \pm 0.14$
4.7 – 6.5	$-0.73 \pm 0.29 \pm 0.27$	$-0.15 \pm 0.31 \pm 0.10$	$-0.73 \pm 0.30 \pm 0.13$
6.5 – 8.5	$-0.32 \pm 0.27 \pm 0.06$	$-0.49 \pm 0.31 \pm 0.10$	$-0.40 \pm 0.36 \pm 0.17$
8.5 – 25.0	$-0.48 \pm 0.17 \pm 0.08$	$-0.32 \pm 0.26 \pm 0.10$	$-0.74 \pm 0.39 \pm 0.09$

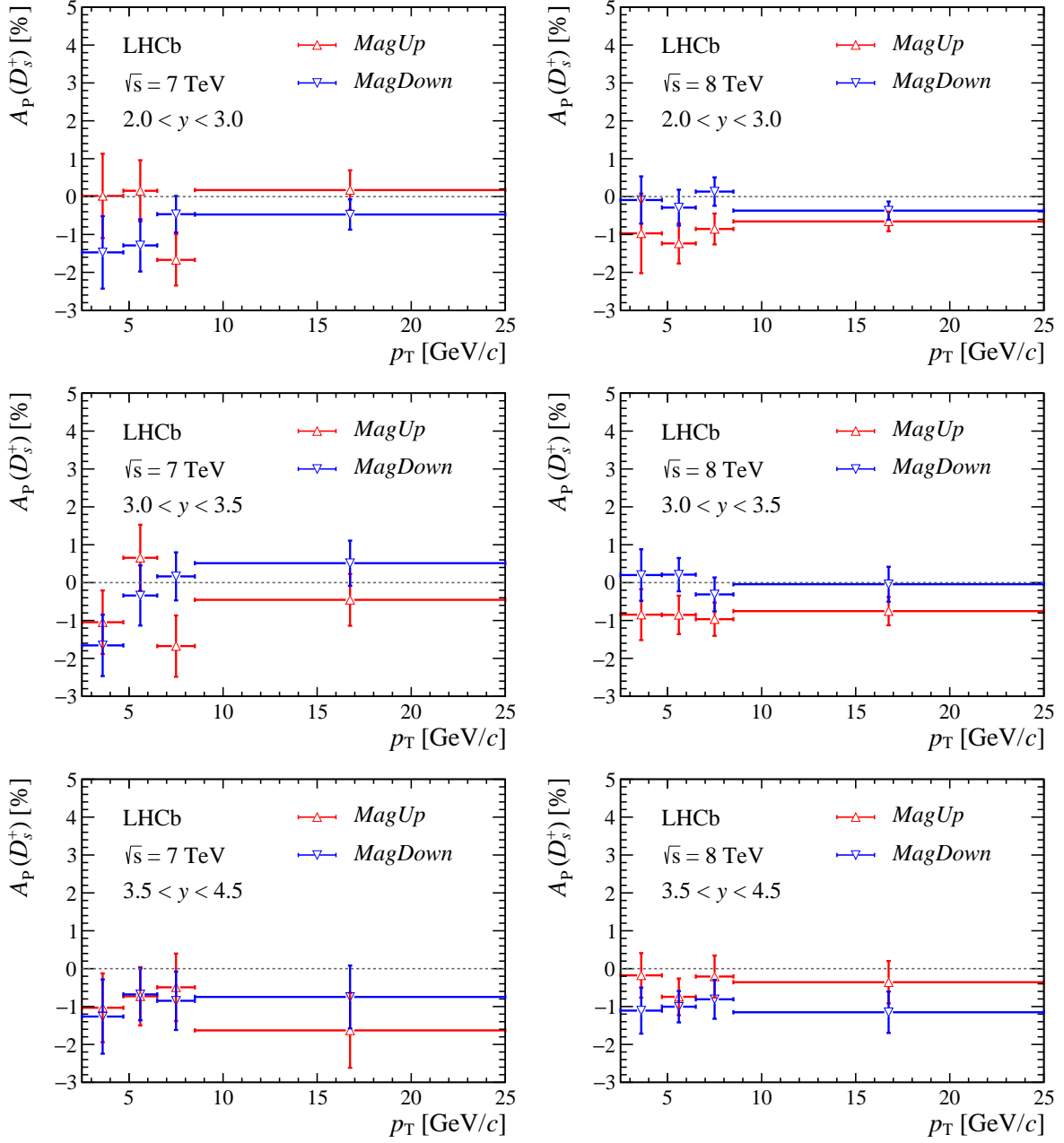


Figure 4: Results of the LHCb measurement of the D_s^+ production asymmetry as a function of p_T for three different bins of rapidity for the (left) $\sqrt{s} = 7$ TeV and (right) 8 TeV data sets, split between the magnet polarities *MagUp* and *MagDown*.

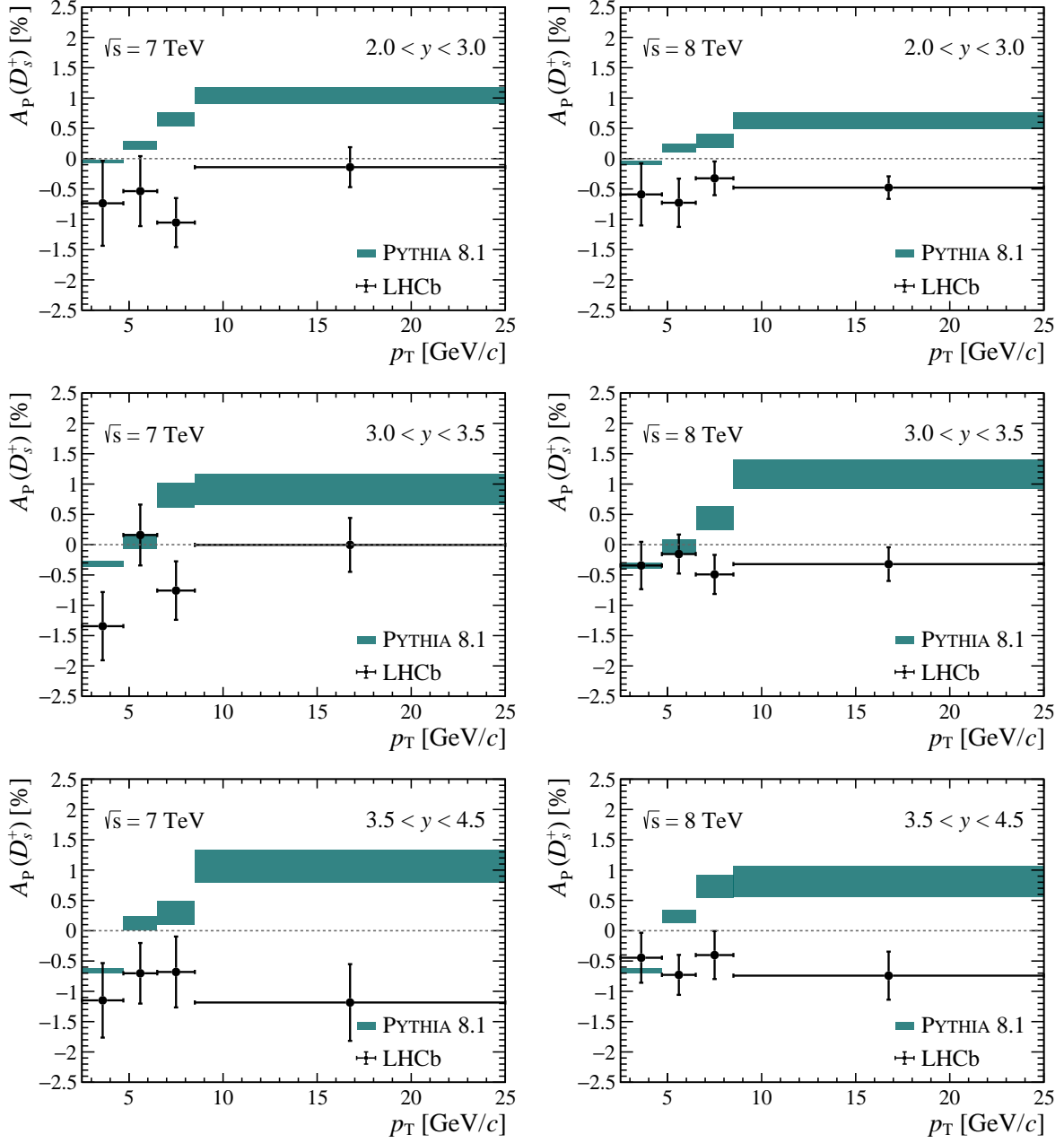


Figure 5: Results of the LHCb measurement of the D_s^+ production asymmetry as a function of p_T for three different bins of rapidity for the (left) $\sqrt{s} = 7$ TeV and (right) 8 TeV data sets, compared to the results from PYTHIA. The uncertainties of the PYTHIA prediction are statistical only.

References

- [1] LHCb collaboration, R. Aaij *et al.*, *Prompt charm production in pp collisions at $\sqrt{s} = 7$ TeV*, Nucl. Phys. **B871** (2013) 1, [arXiv:1302.2864](#).
- [2] B. Andersson, G. Gustafson, G. Ingelman, and T. Sjöstrand, *Parton fragmentation and string dynamics*, Phys. Rept. **97** (1983) 31.
- [3] T. Sjöstrand, S. Mrenna, and P. Skands, *A brief introduction to PYTHIA 8.1*, Comput. Phys. Commun. **178** (2008) 852, [arXiv:0710.3820](#); T. Sjöstrand, S. Mrenna, and P. Skands, *PYTHIA 6.4 physics and manual*, JHEP **05** (2006) 026, [arXiv:hep-ph/0603175](#).
- [4] E. Norrbin, *Heavy quark production asymmetries*, in *Proceedings of EPS-HEP*, p. 408, 1999. [arXiv:hep-ph/9909437](#).
- [5] E. Norrbin and R. Vogt, *Bottom production asymmetries at the LHC*, in *Proceeding of Fifth workshop on electronics for LHC experiments*, 2000. [arXiv:hep-ph/0003056](#).
- [6] E. Norrbin and T. Sjöstrand, *Production and hadronization of heavy quarks*, Eur. Phys. J. **C17** (2000) 137, [arXiv:hep-ph/0005110](#).
- [7] LHCb collaboration, R. Aaij *et al.*, *Measurement of the $D_s^+ - D_s^-$ production asymmetry in 7 TeV pp collisions*, Phys. Lett. **B713** (2012) 186, [arXiv:1205.0897](#).
- [8] LHCb collaboration, A. A. Alves Jr. *et al.*, *The LHCb detector at the LHC*, JINST **3** (2008) S08005.
- [9] LHCb collaboration, R. Aaij *et al.*, *LHCb detector performance*, Int. J. Mod. Phys. **A30** (2015) 1530022, [arXiv:1412.6352](#).
- [10] R. Aaij *et al.*, *The LHCb trigger and its performance in 2011*, JINST **8** (2013) P04022, [arXiv:1211.3055](#).
- [11] I. Belyaev *et al.*, *Handling of the generation of primary events in Gauss, the LHCb simulation framework*, J. Phys. Conf. Ser. **331** (2011) 032047.
- [12] D. J. Lange, *The EvtGen particle decay simulation package*, Nucl. Instrum. Meth. **A462** (2001) 152.
- [13] P. Golonka and Z. Was, *PHOTOS Monte Carlo: A precision tool for QED corrections in Z and W decays*, Eur. Phys. J. **C45** (2006) 97, [arXiv:hep-ph/0506026](#).
- [14] Geant4 collaboration, J. Allison *et al.*, *Geant4 developments and applications*, IEEE Trans. Nucl. Sci. **53** (2006) 270; Geant4 collaboration, S. Agostinelli *et al.*, *Geant4: A simulation toolkit*, Nucl. Instrum. Meth. **A506** (2003) 250.
- [15] M. Clemencic *et al.*, *The LHCb simulation application, Gauss: Design, evolution and experience*, J. Phys. Conf. Ser. **331** (2011) 032023.
- [16] Particle Data Group, C. Patrignani *et al.*, *Review of particle physics*, Chin. Phys. **C40** (2016) 100001, and 2017 update.

- [17] D. Martínez Santos and F. Dupertuis, *Mass distributions marginalized over per-event errors*, Nucl. Instrum. Meth. **A764** (2014) 150, [arXiv:1312.5000](#).
- [18] LHCb collaboration, R. Aaij *et al.*, *Measurement of B meson production cross-sections in proton-proton collisions at $\sqrt{s} = 7$ TeV*, JHEP **08** (2013) 117, [arXiv:1306.3663](#).
- [19] LHCb collaboration, R. Aaij *et al.*, *Study of the kinematic dependences of Λ_b^0 production in pp collisions and a measurement of the $\Lambda_b^0 \rightarrow \Lambda_c^+ \pi^-$ branching fraction*, JHEP **08** (2014) 143, [arXiv:1405.6842](#).
- [20] LHCb collaboration, R. Aaij *et al.*, *Measurement of the B^\pm production asymmetry and the CP asymmetry in $B^\pm \rightarrow J/\psi K^\pm$ decays*, Phys. Rev. **D95** (2017) 052005, [arXiv:1701.05501](#).
- [21] LHCb collaboration, R. Aaij *et al.*, *Measurement of B^0 , B_s^0 , B^+ and Λ_b^0 production asymmetries in 7 and 8 TeV pp collisions*, Phys. Lett. **B774** (2017) 139, [arXiv:1703.08464](#).
- [22] LHCb collaboration, R. Aaij *et al.*, *Measurement of the semileptonic CP asymmetry in $B^0-\bar{B}^0$ mixing*, Phys. Rev. Lett. **114** (2015) 041601, [arXiv:1409.8586](#).
- [23] LHCb collaboration, R. Aaij *et al.*, *Measurement of CP asymmetry in $D^0 \rightarrow K^- K^+$ and $D^0 \rightarrow \pi^- \pi^+$ decays*, JHEP **07** (2014) 041, [arXiv:1405.2797](#).
- [24] LHCb collaboration, R. Aaij *et al.*, *Measurement of the CP asymmetry in $B_s^0-\bar{B}_s^0$ mixing*, Phys. Rev. Lett. **117** (2016) 061803, [arXiv:1605.09768](#).
- [25] LHCb collaboration, R. Aaij *et al.*, *Measurement of the track reconstruction efficiency at LHCb*, JINST **10** (2015) P02007, [arXiv:1408.1251](#).
- [26] L. Anderlini *et al.*, *The PIDCalib package*, LHCb-PUB-2016-021.
- [27] H.-L. Lai *et al.*, *Parton distributions for event generators*, JHEP **04** (2010) 035, [arXiv:0910.4183](#).

LHCb collaboration

R. Aaij⁴³, B. Adeva³⁹, M. Adinolfi⁴⁸, Z. Ajaltouni⁵, S. Akar⁵⁹, P. Albicocco¹⁸, J. Albrecht¹⁰, F. Alessio⁴⁰, M. Alexander⁵³, A. Alfonso Alberio³⁸, S. Ali⁴³, G. Alkhazov³¹, P. Alvarez Cartelle⁵⁵, A.A. Alves Jr⁵⁹, S. Amato², S. Amerio²³, Y. Amhis⁷, L. An³, L. Anderlini¹⁷, G. Andreassi⁴¹, M. Andreotti^{16,g}, J.E. Andrews⁶⁰, R.B. Appleby⁵⁶, F. Archilli⁴³, P. d'Argent¹², J. Arnau Romeu⁶, A. Artamonov³⁷, M. Artuso⁶¹, E. Aslanides⁶, M. Atzeni⁴², G. Auriemma²⁶, S. Bachmann¹², J.J. Back⁵⁰, S. Baker⁵⁵, V. Balagura^{7,b}, W. Baldini¹⁶, A. Baranov³⁵, R.J. Barlow⁵⁶, S. Barsuk⁷, W. Barter⁵⁶, F. Baryshnikov³², V. Batozskaya²⁹, V. Battista⁴¹, A. Bay⁴¹, J. Beddow⁵³, F. Bedeschi²⁴, I. Bediaga¹, A. Beiter⁶¹, L.J. Bel⁴³, N. Bely⁶³, V. Bellec⁴¹, N. Belloli^{20,i}, K. Belous³⁷, I. Belyaev^{32,40}, E. Ben-Haim⁸, G. Bencivenni¹⁸, S. Benson⁴³, S. Beranek⁹, A. Berezhnoy³³, R. Bernet⁴², D. Berninghoff¹², E. Bertholet⁸, A. Bertolin²³, C. Betancourt⁴², F. Betti^{15,40}, M.O. Bettler⁴⁹, M. van Beuzekom⁴³, I.a. Bezshyiko⁴², S. Bifani⁴⁷, P. Billoir⁸, A. Birnkraut¹⁰, A. Bizzeti^{17,u}, M. Björn⁵⁷, T. Blake⁵⁰, F. Blanc⁴¹, S. Blusk⁶¹, V. Bocci²⁶, O. Boente Garcia³⁹, T. Boettcher⁵⁸, A. Bondar^{36,w}, N. Bondar³¹, S. Borghi^{56,40}, M. Borisyak³⁵, M. Borsato^{39,40}, F. Bossu⁷, M. Boubdir⁹, T.J.V. Bowcock⁵⁴, E. Bowen⁴², C. Bozzi^{16,40}, S. Braun¹², M. Brodski⁴⁰, J. Brodzicka²⁷, D. Brundu²², E. Buchanan⁴⁸, C. Burr⁵⁶, A. Bursche²², J. Buytaert⁴⁰, W. Byczynski⁴⁰, S. Cadeddu²², H. Cai⁶⁴, R. Calabrese^{16,g}, R. Calladine⁴⁷, M. Calvi^{20,i}, M. Calvo Gomez^{38,m}, A. Camboni^{38,m}, P. Campana¹⁸, D.H. Campora Perez⁴⁰, L. Capriotti⁵⁶, A. Carbone^{15,e}, G. Carboni²⁵, R. Cardinale^{19,h}, A. Cardini²², P. Carniti^{20,i}, L. Carson⁵², K. Carvalho Akiba², G. Casse⁵⁴, L. Cassina²⁰, M. Cattaneo⁴⁰, G. Cavallero^{19,h}, R. Cenci^{24,p}, D. Chamont⁷, M.G. Chapman⁴⁸, M. Charles⁸, Ph. Charpentier⁴⁰, G. Chatzikonstantinidis⁴⁷, M. Chefdeville⁴, S. Chen²², S.-G. Chitic⁴⁰, V. Chobanova³⁹, M. Chruszcz⁴⁰, A. Chubykin³¹, P. Ciambrone¹⁸, X. Cid Vidal³⁹, G. Ciezarek⁴⁰, P.E.L. Clarke⁵², M. Clemencic⁴⁰, H.V. Cliff⁴⁹, J. Closier⁴⁰, V. Coco⁴⁰, J. Cogan⁶, E. Cogneras⁵, V. Cogoni^{22,f}, L. Cojocariu³⁰, P. Collins⁴⁰, T. Colombo⁴⁰, A. Comerma-Montells¹², A. Contu²², G. Coombs⁴⁰, S. Coquereau³⁸, G. Corti⁴⁰, M. Corvo^{16,g}, C.M. Costa Sobral⁵⁰, B. Couturier⁴⁰, G.A. Cowan⁵², D.C. Craik⁵⁸, A. Crocombe⁵⁰, M. Cruz Torres¹, R. Currie⁵², C. D'Ambrosio⁴⁰, F. Da Cunha Marinho², C.L. Da Silva⁷³, E. Dall'Occo⁴³, J. Dalseno⁴⁸, A. Danilina³², A. Davis³, O. De Aguiar Francisco⁴⁰, K. De Bruyn⁴⁰, S. De Capua⁵⁶, M. De Cian⁴¹, J.M. De Miranda¹, L. De Paula², M. De Serio^{14,d}, P. De Simone¹⁸, C.T. Dean⁵³, D. Decamp⁴, L. Del Buono⁸, B. Delaney⁴⁹, H.-P. Dembinski¹¹, M. Demmer¹⁰, A. Dendek²⁸, D. Derkach³⁵, O. Deschamps⁵, F. Dettori⁵⁴, B. Dey⁶⁵, A. Di Canto⁴⁰, P. Di Nezza¹⁸, S. Didenko⁶⁹, H. Dijkstra⁴⁰, F. Dordei⁴⁰, M. Dorigo⁴⁰, A. Dosil Suárez³⁹, L. Douglas⁵³, A. Dovbnya⁴⁵, K. Dreimanis⁵⁴, L. Dufour⁴³, G. Dujany⁸, P. Durante⁴⁰, J.M. Durham⁷³, D. Dutta⁵⁶, R. Dzhelyadin³⁷, M. Dziwiecek¹², A. Dziurda⁴⁰, A. Dzyuba³¹, S. Easo⁵¹, U. Egede⁵⁵, V. Egorychev³², S. Eidelman^{36,w}, S. Eisenhardt⁵², U. Eitschberger¹⁰, R. Ekelhof¹⁰, L. Eklund⁵³, S. Ely⁶¹, A. Ene³⁰, S. Escher⁹, S. Esen⁴³, H.M. Evans⁴⁹, T. Evans⁵⁷, A. Falabella¹⁵, N. Farley⁴⁷, S. Farry⁵⁴, D. Fazzini^{20,40,i}, L. Federici²⁵, G. Fernandez³⁸, P. Fernandez Declara⁴⁰, A. Fernandez Prieto³⁹, F. Ferrari¹⁵, L. Ferreira Lopes⁴¹, F. Ferreira Rodrigues², M. Ferro-Luzzi⁴⁰, S. Filippov³⁴, R.A. Fini¹⁴, M. Fiorini^{16,g}, M. Firlej²⁸, C. Fitzpatrick⁴¹, T. Fiutowski²⁸, F. Fleuret^{7,b}, M. Fontana^{22,40}, F. Fontanelli^{19,h}, R. Forty⁴⁰, V. Franco Lima⁵⁴, M. Frank⁴⁰, C. Frei⁴⁰, J. Fu^{21,g}, W. Funk⁴⁰, C. Färber⁴⁰, E. Gabriel⁵², A. Gallas Torreira³⁹, D. Galli^{15,e}, S. Gallorini²³, S. Gambetta⁵², M. Gandelman², P. Gandini²¹, Y. Gao³, L.M. Garcia Martin⁷¹, B. Garcia Plana³⁹, J. García Pardiñas⁴², J. Garra Tico⁴⁹, L. Garrido³⁸, D. Gascon³⁸, C. Gaspar⁴⁰, L. Gavardi¹⁰, G. Gazzoni⁵, D. Gerick¹², E. Gersabeck⁵⁶, M. Gersabeck⁵⁶, T. Gershon⁵⁰, Ph. Ghez⁴, S. Giani⁴¹, V. Gibson⁴⁹, O.G. Girard⁴¹, L. Giubega³⁰, K. Gizdov⁵², V.V. Gligorov⁸, D. Golubkov³², A. Golutvin^{55,69}, A. Gomes^{1,a}, I.V. Gorelov³³, C. Gotti^{20,i}, E. Govorkova⁴³, J.P. Grabowski¹², R. Graciani Diaz³⁸, L.A. Granado Cardoso⁴⁰, E. Graugés³⁸, E. Graverini⁴², G. Graziani¹⁷, A. Greco³⁰, R. Greim⁴³,

P. Griffith²², L. Grillo⁵⁶, L. Gruber⁴⁰, B.R. Gruberg Cazon⁵⁷, O. Grünberg⁶⁷, E. Gushchin³⁴,
 Yu. Guz^{37,40}, T. Gys⁴⁰, C. Göbel⁶², T. Hadavizadeh⁵⁷, C. Hadjivasiliou⁵, G. Haefeli⁴¹,
 C. Haen⁴⁰, S.C. Haines⁴⁹, B. Hamilton⁶⁰, X. Han¹², T.H. Hancock⁵⁷, S. Hansmann-Menzemer¹²,
 N. Harnew⁵⁷, S.T. Harnew⁴⁸, C. Hasse⁴⁰, M. Hatch⁴⁰, J. He⁶³, M. Hecker⁵⁵, K. Heinicke¹⁰,
 A. Heister⁹, K. Hennessy⁵⁴, L. Henry⁷¹, E. van Herwijnen⁴⁰, M. Heß⁶⁷, A. Hicheur², D. Hill⁵⁷,
 P.H. Hopchev⁴¹, W. Hu⁶⁵, W. Huang⁶³, Z.C. Huard⁵⁹, W. Hulsbergen⁴³, T. Humair⁵⁵,
 M. Hushchyn³⁵, D. Hutchcroft⁵⁴, P. Ibis¹⁰, M. Idzik²⁸, P. Ilten⁴⁷, K. Ivshin³¹, R. Jacobsson⁴⁰,
 J. Jalocha⁵⁷, E. Jans⁴³, A. Jawahery⁶⁰, F. Jiang³, M. John⁵⁷, D. Johnson⁴⁰, C.R. Jones⁴⁹,
 C. Joram⁴⁰, B. Jost⁴⁰, N. Jurik⁵⁷, S. Kandybei⁴⁵, M. Karacson⁴⁰, J.M. Kariuki⁴⁸, S. Karodia⁵³,
 N. Kazeev³⁵, M. Kecke¹², F. Keizer⁴⁹, M. Kelsey⁶¹, M. Kenzie⁴⁹, T. Ketel⁴⁴, E. Khairullin³⁵,
 B. Khanji¹², C. Khurewathanakul⁴¹, K.E. Kim⁶¹, T. Kirn⁹, S. Klaver¹⁸, K. Klimaszewski²⁹,
 T. Klimkovich¹¹, S. Koliiev⁴⁶, M. Kolpin¹², R. Kopečna¹², P. Koppenburg⁴³, S. Kotriakhova³¹,
 M. Kozeiha⁵, L. Kravchuk³⁴, M. Kreps⁵⁰, F. Kress⁵⁵, P. Krokovny^{36,w}, W. Krupa²⁸,
 W. Krzemien²⁹, W. Kucewicz^{27,l}, M. Kucharczyk²⁷, V. Kudryavtsev^{36,w}, A.K. Kuonen⁴¹,
 T. Kvaratskheliya^{32,40}, D. Lacarrere⁴⁰, G. Lafferty⁵⁶, A. Lai²², G. Lanfranchi¹⁸,
 C. Langenbruch⁹, T. Latham⁵⁰, C. Lazzeroni⁴⁷, R. Le Gac⁶, A. Leflat^{33,40}, J. Lefrançois⁷,
 R. Lefèvre⁵, F. Lemaitre⁴⁰, O. Leroy⁶, T. Lesiak²⁷, B. Leverington¹², P.-R. Li⁶³, T. Li³, Z. Li⁶¹,
 X. Liang⁶¹, T. Likhomanenko⁶⁸, R. Lindner⁴⁰, F. Lionetto⁴², V. Lisovskyi⁷, X. Liu³, D. Loh⁵⁰,
 A. Loi²², I. Longstaff⁵³, J.H. Lopes², D. Lucchesi^{23,o}, M. Lucio Martinez³⁹, A. Lupato²³,
 E. Luppi^{16,g}, O. Lupton⁴⁰, A. Lusiani²⁴, X. Lyu⁶³, F. Machefert⁷, F. Maciuc³⁰, V. Macko⁴¹,
 P. Mackowiak¹⁰, S. Maddrell-Mander⁴⁸, O. Maev^{31,40}, K. Maguire⁵⁶, D. Maisuzenko³¹,
 M.W. Majewski²⁸, S. Malde⁵⁷, B. Malecki²⁷, A. Malinin⁶⁸, T. Maltsev^{36,w}, G. Manca^{22,f},
 G. Mancinelli⁶, D. Marangotto^{21,q}, J. Maratas^{5,v}, J.F. Marchand⁴, U. Marconi¹⁵,
 C. Marin Benito³⁸, M. Marinangeli⁴¹, P. Marino⁴¹, J. Marks¹², G. Martellotti²⁶, M. Martin⁶,
 M. Martinelli⁴¹, D. Martinez Santos³⁹, F. Martinez Vidal⁷¹, A. Massafferri¹, R. Matev⁴⁰,
 A. Mathad⁵⁰, Z. Mathe⁴⁰, C. Matteuzzi²⁰, A. Mauri⁴², E. Maurice^{7,b}, B. Maurin⁴¹,
 A. Mazurov⁴⁷, M. McCann^{55,40}, A. McNab⁵⁶, R. McNulty¹³, J.V. Mead⁵⁴, B. Meadows⁵⁹,
 C. Meaux⁶, F. Meier¹⁰, N. Meinert⁶⁷, D. Melnychuk²⁹, M. Merk⁴³, A. Merli^{21,q}, E. Michielin²³,
 D.A. Milanes⁶⁶, E. Millard⁵⁰, M.-N. Minard⁴, L. Minzoni^{16,g}, D.S. Mitzel¹², A. Mogini⁸,
 J. Molina Rodriguez^{1,y}, T. Mombächer¹⁰, I.A. Monroy⁶⁶, S. Monteil⁵, M. Morandin²³,
 G. Morello¹⁸, M.J. Morello^{24,t}, O. Morgunova⁶⁸, J. Moron²⁸, A.B. Morris⁶, R. Mountain⁶¹,
 F. Muheim⁵², M. Mulder⁴³, D. Müller⁴⁰, J. Müller¹⁰, K. Müller⁴², V. Müller¹⁰, P. Naik⁴⁸,
 T. Nakada⁴¹, R. Nandakumar⁵¹, A. Nandi⁵⁷, I. Nasteva², M. Needham⁵², N. Neri²¹,
 S. Neubert¹², N. Neufeld⁴⁰, M. Neuner¹², T.D. Nguyen⁴¹, C. Nguyen-Mau^{41,n}, S. Nieswand⁹,
 R. Niet¹⁰, N. Nikitin³³, A. Nogay⁶⁸, D.P. O'Hanlon¹⁵, A. Oblakowska-Mucha²⁸, V. Obraztsov³⁷,
 S. Ogilvy¹⁸, R. Oldeman^{22,f}, C.J.G. Onderwater⁷², A. Ossowska²⁷, J.M. Otalora Goicochea²,
 P. Owen⁴², A. Oyanguren⁷¹, P.R. Pais⁴¹, A. Palano¹⁴, M. Palutan^{18,40}, G. Panshin⁷⁰,
 A. Papanestis⁵¹, M. Pappagallo⁵², L.L. Pappalardo^{16,g}, W. Parker⁶⁰, C. Parkes⁵⁶,
 G. Passaleva^{17,40}, A. Pastore¹⁴, M. Patel⁵⁵, C. Patrignani^{15,e}, A. Pearce⁴⁰, A. Pellegrino⁴³,
 G. Penso²⁶, M. Pepe Altarelli⁴⁰, S. Perazzini⁴⁰, D. Pereima³², P. Perret⁵, L. Pescatore⁴¹,
 K. Petridis⁴⁸, A. Petrolini^{19,h}, A. Petrov⁶⁸, M. Petruzzo^{21,q}, B. Pietrzyk⁴, G. Pietrzyk⁴¹,
 M. Pikiés²⁷, D. Pinci²⁶, F. Pisani⁴⁰, A. Pistone^{19,h}, A. Piucci¹², V. Placinta³⁰, S. Playfer⁵²,
 M. Plo Casasus³⁹, F. Polci⁸, M. Poli Lener¹⁸, A. Poluektov⁵⁰, N. Polukhina^{69,c}, I. Polyakov⁶¹,
 E. Polcarpo², G.J. Pomery⁴⁸, S. Ponce⁴⁰, A. Popov³⁷, D. Popov^{11,40}, S. Poslavskii³⁷,
 C. Potterat², E. Price⁴⁸, J. Prisciandaro³⁹, C. Prouve⁴⁸, V. Pugatch⁴⁶, A. Puig Navarro⁴²,
 H. Pullen⁵⁷, G. Punzi^{24,p}, W. Qian⁶³, J. Qin⁶³, R. Quagliani⁸, B. Quintana⁵, B. Rachwal²⁸,
 J.H. Rademacker⁴⁸, M. Rama²⁴, M. Ramos Pernas³⁹, M.S. Rangel², F. Ratnikov^{35,x},
 G. Raven⁴⁴, M. Ravonel Salzgeber⁴⁰, M. Reboud⁴, F. Redi⁴¹, S. Reichert¹⁰, A.C. dos Reis¹,
 C. Remon Alepuz⁷¹, V. Renaudin⁷, S. Ricciardi⁵¹, S. Richards⁴⁸, K. Rinnert⁵⁴, P. Robbe⁷,
 A. Robert⁸, A.B. Rodrigues⁴¹, E. Rodrigues⁵⁹, J.A. Rodriguez Lopez⁶⁶, A. Rogozhnikov³⁵,

S. Roiser⁴⁰, A. Rollings⁵⁷, V. Romanovskiy³⁷, A. Romero Vidal^{39,40}, M. Rotondo¹⁸, M.S. Rudolph⁶¹, T. Ruf⁴⁰, J. Ruiz Vidal⁷¹, J.J. Saborido Silva³⁹, N. Sagidova³¹, B. Saitta^{22,f}, V. Salustino Guimaraes⁶², C. Sanchez Mayordomo⁷¹, B. Sanmartin Sedes³⁹, R. Santacesaria²⁶, C. Santamarina Rios³⁹, M. Santimaria¹⁸, E. Santovetti^{25,j}, G. Sarpis⁵⁶, A. Sarti^{18,k}, C. Satriano^{26,s}, A. Satta²⁵, D. Savrina^{32,33}, S. Schael⁹, M. Schellenberg¹⁰, M. Schiller⁵³, H. Schindler⁴⁰, M. Schmelling¹¹, T. Schmelzer¹⁰, B. Schmidt⁴⁰, O. Schneider⁴¹, A. Schopper⁴⁰, H.F. Schreiner⁵⁹, M. Schubiger⁴¹, M.H. Schune⁷, R. Schwemmer⁴⁰, B. Sciascia¹⁸, A. Sciubba^{26,k}, A. Semennikov³², E.S. Sepulveda⁸, A. Sergi^{47,40}, N. Serra⁴², J. Serrano⁶, L. Sestini²³, P. Seyfert⁴⁰, M. Shapkin³⁷, Y. Shcheglov^{31,†}, T. Shears⁵⁴, L. Shekhtman^{36,w}, V. Shevchenko⁶⁸, B.G. Siddi¹⁶, R. Silva Coutinho⁴², L. Silva de Oliveira², G. Simi^{23,o}, S. Simone^{14,d}, N. Skidmore¹², T. Skwarnicki⁶¹, I.T. Smith⁵², M. Smith⁵⁵, I. Soares Lavra¹, M.D. Sokoloff⁵⁹, F.J.P. Soler⁵³, B. Souza De Paula², B. Spaan¹⁰, P. Spradlin⁵³, F. Stagni⁴⁰, M. Stahl¹², S. Stahl⁴⁰, P. Stefko⁴¹, S. Stefkova⁵⁵, O. Steinkamp⁴², S. Stemmler¹², O. Stenyakin³⁷, M. Stepanova³¹, H. Stevens¹⁰, S. Stone⁶¹, B. Storaci⁴², S. Stracka^{24,p}, M.E. Stramaglia⁴¹, M. Straticiuc³⁰, U. Straumann⁴², S. Strokov⁷⁰, J. Sun³, L. Sun⁶⁴, K. Swientek²⁸, V. Syropoulos⁴⁴, T. Szumlak²⁸, M. Szymanski⁶³, S. T’Jampens⁴, Z. Tang³, A. Tayduganov⁶, T. Tekampe¹⁰, G. Tellarini¹⁶, F. Teubert⁴⁰, E. Thomas⁴⁰, J. van Tilburg⁴³, M.J. Tilley⁵⁵, V. Tisserand⁵, M. Tobin⁴¹, S. Tolk⁴⁰, L. Tomassetti^{16,g}, D. Tonelli²⁴, R. Tourinho Jadallah Aoude¹, E. Tournefier⁴, M. Traill⁵³, M.T. Tran⁴¹, M. Tresch⁴², A. Trisovic⁴⁹, A. Tsaregorodtsev⁶, A. Tully⁴⁹, N. Tuning^{43,40}, A. Ukleja²⁹, A. Usachov⁷, A. Ustyuzhanin³⁵, U. Uwer¹², C. Vacca^{22,f}, A. Vagner⁷⁰, V. Vagnoni¹⁵, A. Valassi⁴⁰, S. Valat⁴⁰, G. Valenti¹⁵, R. Vazquez Gomez⁴⁰, P. Vazquez Regueiro³⁹, S. Vecchi¹⁶, M. van Veghel⁴³, J.J. Velthuis⁴⁸, M. Veltri^{17,r}, G. Veneziano⁵⁷, A. Venkateswaran⁶¹, T.A. Verlage⁹, M. Vernet⁵, M. Vesterinen⁵⁷, J.V. Viana Barbosa⁴⁰, D. Vieira⁶³, M. Vieites Diaz³⁹, H. Viemann⁶⁷, X. Vilasis-Cardona^{38,m}, A. Vitkovskiy⁴³, M. Vitti⁴⁹, V. Volkov³³, A. Vollhardt⁴², B. Voneki⁴⁰, A. Vorobyev³¹, V. Vorobyev^{36,w}, C. Voß⁹, J.A. de Vries⁴³, C. Vázquez Sierra⁴³, R. Waldi⁶⁷, J. Walsh²⁴, J. Wang⁶¹, M. Wang³, Y. Wang⁶⁵, Z. Wang⁴², D.R. Ward⁴⁹, H.M. Wark⁵⁴, N.K. Watson⁴⁷, D. Websdale⁵⁵, A. Weiden⁴², C. Weisser⁵⁸, M. Whitehead⁹, J. Wicht⁵⁰, G. Wilkinson⁵⁷, M. Wilkinson⁶¹, M.R.J. Williams⁵⁶, M. Williams⁵⁸, T. Williams⁴⁷, F.F. Wilson^{51,40}, J. Wimberley⁶⁰, M. Winn⁷, J. Wishahi¹⁰, W. Wislicki²⁹, M. Witek²⁷, G. Wormser⁷, S.A. Wotton⁴⁹, K. Wyllie⁴⁰, D. Xiao⁶⁵, Y. Xie⁶⁵, A. Xu³, M. Xu⁶⁵, Q. Xu⁶³, Z. Xu³, Z. Xu⁴, Z. Yang³, Z. Yang⁶⁰, Y. Yao⁶¹, H. Yin⁶⁵, J. Yu⁶⁵, X. Yuan⁶¹, O. Yushchenko³⁷, K.A. Zarebski⁴⁷, M. Zavertyaev^{11,c}, L. Zhang³, W.C. Zhang^{3,z}, Y. Zhang⁷, A. Zhelezov¹², Y. Zheng⁶³, X. Zhu³, V. Zhukov^{9,33}, J.B. Zonneveld⁵², S. Zucchelli¹⁵.

¹ Centro Brasileiro de Pesquisas Físicas (CBPF), Rio de Janeiro, Brazil

² Universidade Federal do Rio de Janeiro (UFRJ), Rio de Janeiro, Brazil

³ Center for High Energy Physics, Tsinghua University, Beijing, China

⁴ Univ. Grenoble Alpes, Univ. Savoie Mont Blanc, CNRS, IN2P3-LAPP, Annecy, France

⁵ Clermont Université, Université Blaise Pascal, CNRS/IN2P3, LPC, Clermont-Ferrand, France

⁶ Aix Marseille Univ, CNRS/IN2P3, CPPM, Marseille, France

⁷ LAL, Univ. Paris-Sud, CNRS/IN2P3, Université Paris-Saclay, Orsay, France

⁸ LPNHE, Université Pierre et Marie Curie, Université Paris Diderot, CNRS/IN2P3, Paris, France

⁹ I. Physikalisches Institut, RWTH Aachen University, Aachen, Germany

¹⁰ Fakultät Physik, Technische Universität Dortmund, Dortmund, Germany

¹¹ Max-Planck-Institut für Kernphysik (MPIK), Heidelberg, Germany

¹² Physikalisches Institut, Ruprecht-Karls-Universität Heidelberg, Heidelberg, Germany

¹³ School of Physics, University College Dublin, Dublin, Ireland

¹⁴ INFN Sezione di Bari, Bari, Italy

¹⁵ INFN Sezione di Bologna, Bologna, Italy

¹⁶ INFN Sezione di Ferrara, Ferrara, Italy

¹⁷ INFN Sezione di Firenze, Firenze, Italy

- ¹⁸ INFN Laboratori Nazionali di Frascati, Frascati, Italy
- ¹⁹ INFN Sezione di Genova, Genova, Italy
- ²⁰ INFN Sezione di Milano-Bicocca, Milano, Italy
- ²¹ INFN Sezione di Milano, Milano, Italy
- ²² INFN Sezione di Cagliari, Monserrato, Italy
- ²³ INFN Sezione di Padova, Padova, Italy
- ²⁴ INFN Sezione di Pisa, Pisa, Italy
- ²⁵ INFN Sezione di Roma Tor Vergata, Roma, Italy
- ²⁶ INFN Sezione di Roma La Sapienza, Roma, Italy
- ²⁷ Henryk Niewodniczanski Institute of Nuclear Physics Polish Academy of Sciences, Kraków, Poland
- ²⁸ AGH - University of Science and Technology, Faculty of Physics and Applied Computer Science, Kraków, Poland
- ²⁹ National Center for Nuclear Research (NCBJ), Warsaw, Poland
- ³⁰ Horia Hulubei National Institute of Physics and Nuclear Engineering, Bucharest-Magurele, Romania
- ³¹ Petersburg Nuclear Physics Institute (PNPI), Gatchina, Russia
- ³² Institute of Theoretical and Experimental Physics (ITEP), Moscow, Russia
- ³³ Institute of Nuclear Physics, Moscow State University (SINP MSU), Moscow, Russia
- ³⁴ Institute for Nuclear Research of the Russian Academy of Sciences (INR RAS), Moscow, Russia
- ³⁵ Yandex School of Data Analysis, Moscow, Russia
- ³⁶ Budker Institute of Nuclear Physics (SB RAS), Novosibirsk, Russia
- ³⁷ Institute for High Energy Physics (IHEP), Protvino, Russia
- ³⁸ ICCUB, Universitat de Barcelona, Barcelona, Spain
- ³⁹ Instituto Galego de Física de Altas Enerxías (IGFAE), Universidade de Santiago de Compostela, Santiago de Compostela, Spain
- ⁴⁰ European Organization for Nuclear Research (CERN), Geneva, Switzerland
- ⁴¹ Institute of Physics, Ecole Polytechnique Fédérale de Lausanne (EPFL), Lausanne, Switzerland
- ⁴² Physik-Institut, Universität Zürich, Zürich, Switzerland
- ⁴³ Nikhef National Institute for Subatomic Physics, Amsterdam, The Netherlands
- ⁴⁴ Nikhef National Institute for Subatomic Physics and VU University Amsterdam, Amsterdam, The Netherlands
- ⁴⁵ NSC Kharkiv Institute of Physics and Technology (NSC KIPT), Kharkiv, Ukraine
- ⁴⁶ Institute for Nuclear Research of the National Academy of Sciences (KINR), Kyiv, Ukraine
- ⁴⁷ University of Birmingham, Birmingham, United Kingdom
- ⁴⁸ H.H. Wills Physics Laboratory, University of Bristol, Bristol, United Kingdom
- ⁴⁹ Cavendish Laboratory, University of Cambridge, Cambridge, United Kingdom
- ⁵⁰ Department of Physics, University of Warwick, Coventry, United Kingdom
- ⁵¹ STFC Rutherford Appleton Laboratory, Didcot, United Kingdom
- ⁵² School of Physics and Astronomy, University of Edinburgh, Edinburgh, United Kingdom
- ⁵³ School of Physics and Astronomy, University of Glasgow, Glasgow, United Kingdom
- ⁵⁴ Oliver Lodge Laboratory, University of Liverpool, Liverpool, United Kingdom
- ⁵⁵ Imperial College London, London, United Kingdom
- ⁵⁶ School of Physics and Astronomy, University of Manchester, Manchester, United Kingdom
- ⁵⁷ Department of Physics, University of Oxford, Oxford, United Kingdom
- ⁵⁸ Massachusetts Institute of Technology, Cambridge, MA, United States
- ⁵⁹ University of Cincinnati, Cincinnati, OH, United States
- ⁶⁰ University of Maryland, College Park, MD, United States
- ⁶¹ Syracuse University, Syracuse, NY, United States
- ⁶² Pontifícia Universidade Católica do Rio de Janeiro (PUC-Rio), Rio de Janeiro, Brazil, associated to ²
- ⁶³ University of Chinese Academy of Sciences, Beijing, China, associated to ³
- ⁶⁴ School of Physics and Technology, Wuhan University, Wuhan, China, associated to ³
- ⁶⁵ Institute of Particle Physics, Central China Normal University, Wuhan, Hubei, China, associated to ³
- ⁶⁶ Departamento de Física, Universidad Nacional de Colombia, Bogota, Colombia, associated to ⁸
- ⁶⁷ Institut für Physik, Universität Rostock, Rostock, Germany, associated to ¹²
- ⁶⁸ National Research Centre Kurchatov Institute, Moscow, Russia, associated to ³²
- ⁶⁹ National University of Science and Technology "MISIS", Moscow, Russia, associated to ³²
- ⁷⁰ National Research Tomsk Polytechnic University, Tomsk, Russia, associated to ³²

⁷¹*Instituto de Fisica Corpuscular, Centro Mixto Universidad de Valencia - CSIC, Valencia, Spain, associated to* ³⁸

⁷²*Van Swinderen Institute, University of Groningen, Groningen, The Netherlands, associated to* ⁴³

⁷³*Los Alamos National Laboratory (LANL), Los Alamos, United States, associated to* ⁶¹

^a*Universidade Federal do Triângulo Mineiro (UFTM), Uberaba-MG, Brazil*

^b*Laboratoire Leprince-Ringuet, Palaiseau, France*

^c*P.N. Lebedev Physical Institute, Russian Academy of Science (LPI RAS), Moscow, Russia*

^d*Università di Bari, Bari, Italy*

^e*Università di Bologna, Bologna, Italy*

^f*Università di Cagliari, Cagliari, Italy*

^g*Università di Ferrara, Ferrara, Italy*

^h*Università di Genova, Genova, Italy*

ⁱ*Università di Milano Bicocca, Milano, Italy*

^j*Università di Roma Tor Vergata, Roma, Italy*

^k*Università di Roma La Sapienza, Roma, Italy*

^l*AGH - University of Science and Technology, Faculty of Computer Science, Electronics and Telecommunications, Kraków, Poland*

^m*LIFAELS, La Salle, Universitat Ramon Llull, Barcelona, Spain*

ⁿ*Hanoi University of Science, Hanoi, Vietnam*

^o*Università di Padova, Padova, Italy*

^p*Università di Pisa, Pisa, Italy*

^q*Università degli Studi di Milano, Milano, Italy*

^r*Università di Urbino, Urbino, Italy*

^s*Università della Basilicata, Potenza, Italy*

^t*Scuola Normale Superiore, Pisa, Italy*

^u*Università di Modena e Reggio Emilia, Modena, Italy*

^v*MSU - Iligan Institute of Technology (MSU-IIT), Iligan, Philippines*

^w*Novosibirsk State University, Novosibirsk, Russia*

^x*National Research University Higher School of Economics, Moscow, Russia*

^y*Escuela Agrícola Panamericana, San Antonio de Oriente, Honduras*

^z*School of Physics and Information Technology, Shaanxi Normal University (SNNU), Xi'an, China*

[†]*Deceased*